Crystal structures of Nipah and Hendra virus fusion core proteins

Zhiyong Lou[1,2,*], Yanhui Xu[1,2,*], Kehui Xiang[1], Nan Su[1], Lan Qin[1], Xu Li[1], George F. Gao[3], Mark Bartlam[1,2] and Zihe Rao[1,2,4,*]

1 Tsinghua-Nankai-IBP Joint Research Group for Structural Biology, Tsinghua University, Beijing, China
2 National Laboratory of Biomacromolecules, IBP, Chinese, Academy of Sciences, Beijing, China
3 Center for Molecular Virology, Institute of Microbiology, Chinese Academy of Sciences, Beijing, China
4 Nankai University, Tiangin, China

The Nipah and Hendra viruses are highly pathogenic paramyxoviruses that recently emerged from flying foxes to cause serious disease outbreaks in humans and livestock in Australia, Malaysia, Singapore and Bangladesh. Their unique genetic constitution, high virulence and wide host range set them apart from other paramyxoviruses. These characteristics have led to their classification into the new genus *Henpavirus* within the family Paramyxoviridae and to their designation as Biosafety Level 4 pathogens. The fusion protein, an enveloped glycoprotein essential for viral entry, belongs to the family of class I fusion proteins and is characterized by the presence of two heptad repeat (HR) regions, HR1 and HR2. These two regions associate to form a fusion-active hairpin conformation that juxtaposes the viral and cellular membranes to facilitate membrane fusion and enable subsequent viral entry. The Hendra and Nipah virus fusion core proteins were crystallized and their structures determined to 2.2 Å resolution. The Nipah and Hendra fusion core structures are six-helix bundles with three HR2 helices packed against the hydrophobic grooves on the surface of a central coiled coil formed by three parallel HR1 helices in an oblique antiparallel manner. Because of the high level of conservation in core regions, it is proposed that the Nipah and Hendra virus fusion cores can provide a model for membrane fusion in all paramyxoviruses. The relatively deep grooves on the surface of the central coiled coil represent a good target site for drug discovery strategies aimed at inhibiting viral entry by blocking hairpin formation.

The Nipah virus (NiV) is a newly emerging pathogen identified in 1999 and responsible for the disease transmitted from pigs to humans, killing 105 of its 276 victims [1,2]. This enigmatic, highly lethal group of viruses has struck again this year, with more than 40 people in central Bangladesh falling ill with encephalitis resulting in 14 deaths [3]. The Hendra virus (HeV), an Australian cousin of the Nipah virus, emerged in 1994 and was transmitted to humans from close contact with horses, resulting in two deaths [4]. Both NiV and HeV are unusual among the paramyxoviruses in their abilities to infect and cause potentially fatal disease (encephalitis) in a number of hosts, including human beings [5,6]. These two viruses also have much larger genomes than any other members of the paramyxoviruses [5,7,8]. Phylogenetic analysis of their genomes shows that they are distinct members of the family Paramyxoviridae, but are closely related to members of the genus *Morbillivirus* and the genus *Respirovirus* [7,8]. They have now been grouped into a new genus, *Henipavirus*, inside the family Paramyxoviridae [5,6]. The high mortality rate resulting from these viruses

and their ability to jump species barriers have attracted detailed attention, as they have many of the physical attributes to serve as potential agents of bioterrorism [5,6,9].

Paramyxoviruses are enveloped negative-stranded RNA viruses, forming a large family (Paramyxoviridae) divided into two subfamilies with five established and two newly defined genera (*Rubulavirus*, *Respirovirus*, *Morbillivirus*, *Pneumovirus*, *Metapneumovirus* and the new *Avulavirus* and *Henipavirus*) [6,10,11]. Like other paramyxoviruses, NiV and HeV consist of two surface glycoproteins on the viral surface, termed the fusion (F) protein and glycoprotein (G protein, also called attachment protein) [7,8,12,13]. These two glycoproteins are both responsible for viral fusion and entry into host cells [12,13]. The G protein initiates viral infection by binding to the cellular receptor (attachment), whereas the F protein mediates the subsequent virus–cell membrane fusion process [12–14]. The F protein undergoes a series of conformational changes in the attachment and subsequent fusion process mediated by the paramyxoviruses [14–16].

The F proteins of paramyxoviruses share several features with other viral glycoproteins responsible for membrane fusion, including the hemagglutinin (HA) protein in influenza virus, gp160 of HIV-1, GP of Ebola virus and the spike protein of severe acute respiratory syndrome virus and other coronaviruses. These glycoproteins play a crucial role in the conformational changes during the virus-mediated membrane fusion process [15–20]. They are all initially synthesized as a single-chain precursor, termed F0 in paramyxovirus, which is then cleaved into two subunits (F1 and F2 in paramyxovirus) by a furin-like enzyme derived from the host cell [7]. F1 and F2 are covalently linked by a disulfide bond, and the complex forms a trimer on the virus envelope. The fusion peptide at the N-terminus of F1 is highly hydrophobic and is considered to be responsible for direct insertion of the F protein into the cellular lipid bilayer [15,16,22]. The highly conserved heptad repeat (HR) regions in F1, HR1 and HR2, seemingly act as scaffolding modules. HR1 and HR2 will interact with each other to form a so-called 'trimer of hairpins', 'six-helix bundle' or 'fusion core' in the membrane fusion process. In the fusion core structure, three HR1 helices form a central trimeric coiled coil surrounded by three HR2 helices in an oblique antiparallel manner [15,16,23]. This hairpin formation aligns the transmembrane domain in the viral membrane closely with the fusion peptide inserted into the cellular membrane, thus facilitating membrane fusion.

There are at least three different conformations in the membrane fusion process in the model for the viral fusion mechanism proposed from the gp41 structure of HIV. The first is the native (nonfusogenic) conformation in which the HR1 peptides and HR2 peptides are inaccessible. The subsequent conformation is the prehairpin intermediate, in which the HR1 peptides are exposed with their fusion peptides inserted into the target cellular membrane. The last conformation is the fusogenic state, in which the HR1 and HR2 peptides come together and form a highly stable coiled coil aligning the viral and cellular membranes in juxtaposition, facilitating membrane fusion and viral entry [24]. Introduction of exogenous soluble HR1 or HR2 into the virus infection system will block the formation of this hairpin structure and thus inhibit viral fusion and subsequent infection by competing with the endogenous HR1–HR2 interaction and holding the F protein in the intermediate state [16,25]. Recent studies have shown that the HR2 peptide of NiV and HeV has strong inhibitory activity for membrane fusion in the *in vitro* cell fusion system of the viruses [26]. Our previous biochemical and biophysical studies have also shown that the complex of HR1 and HR2 in NiV or HeV forms a typical thermostable six-helix bundle [21]. However, detailed structures of the complex and the interaction between HR1 and HR2 in NiV or HeV have not been reported to date.

In this study, a single chain combining the HR1 and HR2 peptides (termed the two-helix) was constructed for both NiV and HeV and expressed in the *Escherichia coli* system used previously for other paramyxoviruses [27–33]. We have determined the crystal structures of the NiV two-helix and HeV two-helix to 2.2 Å resolution, thus confirming the formation of a six-helix bundle. These structures also show the typical characteristics of NiV and HeV F proteins as members of the Paramyxoviridae family, and provide a structural basis to explain the inhibitory effects of HR2 on viral fusion and formation of the fusion core structure. The results also show that the HR2 proteins of NiV and HeV are functionally and structurally interchangeable, and this correlates with the sequence similarity of the HR peptides in NiV and HeV (predicted HR1 regions are identical for NiV and HeV but there is a two amino acid difference in the HR2 regions).

Results and Discussion

Structure determination

The HR1 and HR2 regions of the NiV and HeV F proteins consist of residues 137–178 and residues 453–485, respectively, and were predicted by a computer program called LEARNCOIL-VMF [34]. The two

peptides encompassing the N-terminal and C-terminal HRs of the NiV/HeV F protein assemble into a stable trimer of heterodimers [21]. The two-helix molecules were prepared as a single chain by linking HR1 and HR2 with a linker (Fig. 1A). The NiV two-helix forms crystals with unit cell parameters $a = 31.7$ Å, $b = 31.7$ Å, $c = 51.3$ Å, $\alpha = 80.7°$, $\beta = 86.3°$ and $\gamma = 65.8$, and belongs to the space group P1. The crystals contain three two-helix molecules (one stable trimer) per asymmetric unit and diffract to 2.2 Å. The solvent content is estimated to be 21% with a Matthews coefficient (V_m) of 1.5 Å^3·Da^{-1}. The HeV selenomethionyl derivative crystals belong to space group P1 with unit cell parameters $a = 32.0$ Å, $b = 32.0$ Å, $c = 53.9$ Å, $\alpha = 86.0°$, $\beta = 85.8°$ and $\gamma = 68.2$, and diffraction extends to 2.2 Å. Assuming the presence of three two-helix molecules (one stable trimer) per asymmetric unit, the solvent content is estimated to be 26%, with a Matthews coefficient (V_m) of 1.7 Å^3·Da^{-1}. Selected data statistics are shown in Table 1.

The HeV two-helix crystal structure was determined by multiple wavelength anomalous dispersion (MAD) from a single selenomethionyl derivative crystal. Three selenium sites were located in one asymmetric unit from Patterson maps calculated with the program CNS [35]. The model was improved by cycles of manual building and refinement using the programs O [36] and CNS [35]. The structure was subsequently refined to a final R-value of 21.3% and a free R-value of 27.4%.

The NiV two-helix crystal structure was determined by molecular replacement with the HeV two-helix structure as a search model. After rotation and translation function searches with CNS [35], the model was improved by cycles of manual building and refinement using the programs O [36] and CNS [35]. The final R-value and the free R-value for the refinement were 22.5% and 28.0%, respectively.

Overall description of the structure

The three-dimensional structures of NiV and HeV two-helix are very similar, with an rmsd of 1.4 Å for all Cα atoms, which correlates with their high amino acid sequence identity. Unless otherwise stated, we will concentrate on the structure of the NiV two-helix in the following discussion. The fusion core of NiV has a rod-shaped structure approximately 50 Å in length and with a maximum diameter of 28 Å. The NiV two-helix complex structure is a six-helix bundle comprising a trimer of NiV two-helix molecules. The center of this bundle consists of a parallel trimeric coiled coil formed by three HR1 helices, against which three HR2 helices pack in an antiparallel manner (Fig. 2A,B). The
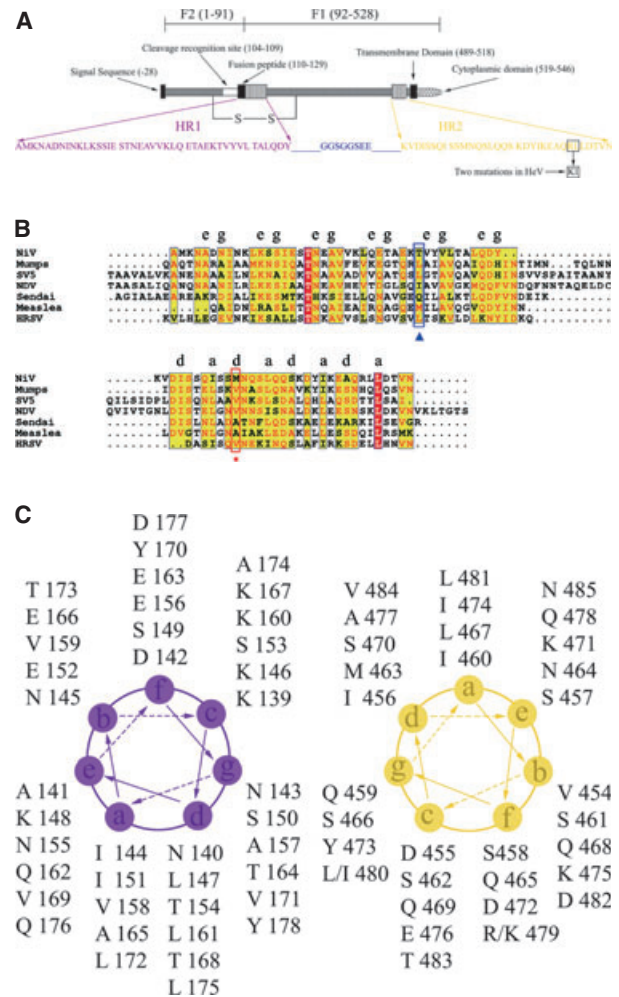
Fig. 1. Construction and sequence alignment of the Nipah virus (NiV) and Hendra virus (HeV) fusion cores. (A) Prediction of the heptad repeat (HR) regions and the construction strategy for the two-helix protein constructs of both NiV and HeV F proteins. A schematic diagram of NiV and HeV F proteins with the location of structurally significant domains is given. The listed sequences of HR1 (137–178) and HR2 (453–485) used in this study were derived from the LEARNCOIL-VMF prediction program. (B) Sequence alignment of paramyxovirus spike protein HR1 and HR2 regions. Residues highlighted with a red background are those that are strictly conserved; residues highlighted with a yellow background are residues that are more than 80% conserved. Residues that are important for HR1 and HR2 interactions, including the e and g positions in HR1 and the a and d positions in HR2, are labeled. Residues that are important in the end deep groove in HR1 and HR2 are framed and labeled with a blue triangle and red star. SV5, parainfluenza virus 5 or simian virus 5; NDV, Newcastle disease virus; HRSV, human respiratory syncytial virus. (C) Helix wheel analysis of the predicted coiled-coil regions of NiV F protein HR1 and HR2, which are represented as purple and golden wheels, respectively. The two substitutions in HeV relative to NiV were located in positions g and f of the helix wheel, not in the a or d positions, which are important for the central HR1 trimer formation. The substitutions of RL to KI are also conservative.

Table 1. Data collection (A) and model refinement (B) statistics.

A.

	HeV two-helix			NiV two-helix
	Peak	Edge	Remote	Native
Wavelength (Å)	0.9799	0.9801	0.9500	1.5418
Space group	P1	P1	P1	P1
Unit cell parameters (Å)	$a = 32.3$ Å,	$a = 32.3$ Å,	$a = 32.2$ Å,	$a = 31.7$ Å,
	$b = 32.5$ Å,	$b = 32.3$ Å,	$b = 32.9$ Å,	$b = 31.7$ Å,
	$c = 54.0$ Å,	$c = 54.0$ Å,	$c = 53.9$ Å,	$c = 51.3$ Å,
	$\alpha = 87.0$ Å,	$\alpha = 86.4$ Å,	$\alpha = 86.3$ Å,	$\alpha = 80.7$ Å,
	$\beta = 86.3$ Å,	$\beta = 86.3$ Å,	$\beta = 86.2$ Å,	$\beta = 86.3$ Å,
	$\gamma = 67.9$ Å	$\gamma = 68.0$ Å	$\gamma = 68.0$ Å	$\gamma = 65.8$ Å
Wavelength (Å)	0.9799	0.9801	0.9500	1.5418
Resolution range (Å)	35.0–2.2	35.0–2.2	35.0–2.2	35.0–2.2
	(2.3–2.2)	(2.3–2.2)	(2.3–2.2)	(2.3–2.2)
Observed reflections	67 673	65 774	62 546	27 810
Unique reflections	9875	9788	9645	8630
Completeness (%)	99.0 (96.7)	99.2 (98.1)	96.1 (94.2)	94.8 (91.0)
I/σ (I)	5.9 (4.9)	5.5 (4.2)	5.1 (4.2)	8.2 (2.8)
R_{merge} (%)	13.4 (37.8)	13.2 (36.5)	14.5 (37.7)	7.1 (37.4)

B.

	HeV two-helix	NiV two-helix
R_{work}	21.3	22.5
R_{free}	27.4	28.0
Resolution range (Å)	35.0–2.2	35.0–2.2
Total reflections used	9484	9317
No. of reflections in working set	8980	8282
No. of reflections in test set	504	434
Average B factor (Å^2)	29.8	31.4
rmsd bonds (Å)	0.008	0.011
rmsd angles (°)	0.962	1.153

N-terminus of HR1 and the C-terminus of HR2 are located at the same end of the six-helix bundle, placing the fusion peptide and transmembrane domains close together. A region of about 270 amino acids would be located at the other end of the six-helix bundle between HR1 and HR2 in the postfusion state of NiV F protein.

The eight amino acids in the linker and several terminal residues were disordered in the electron density map and could not be traced in any of the three molecules. In one asymmetric unit of the NiV structure, the three molecules include residues 143–176 in HR1 and 455–484 in HR2, 143–175 in HR1 and 455–484 in HR2, and 143–175 in HR1 and 458–485 in HR2, respectively. In the HeV structure, the three molecules in one asymmetric unit include residues 143–176 in HR1 and 455–484 in HR2, 143–175 in HR1 and 454–484 in HR2, and 143–177 in HR1 and 457–484 in HR2, respectively. The rmsd of the NiV two-helix and the HeV two-helix is 1.3 Å for all Cα atoms.

Residues 143–176 of HR1 fold into a nine-turn α-helix that extends over the entire length of the coiled coil. As in other naturally occurring coiled coils of the fusion core, the residues in the a and d positions of the fusion core diagram representation [24] of HR1 are predominantly hydrophobic (Fig. 1B). A sequence alignment of NiV with other representative paramyxovirus fusion proteins shows that the residues in these two HR positions are highly conserved (Fig. 1B).

Residues 455–484 of HR2 form an eight-turn amphipathic α-helix stretching the entire length of the coiled coil. Each HR2 peptide packs against the long grooves formed by the interface of the three HR1 helices, and no interaction is observed between individual HR2 helices (Fig. 2A,B). The C-terminus of HR2 ends with V484, which is aligned with N143 of HR1; N143 is also the N-terminus of the HR1 domain. The N-terminus of HR2 starts with I456, which is aligned with L175 of HR1 (Fig. 2C).

A

HR1

HR2

B N143

V484

C V 484

N 143

HR2

N

HR1

C

I 456

L 175
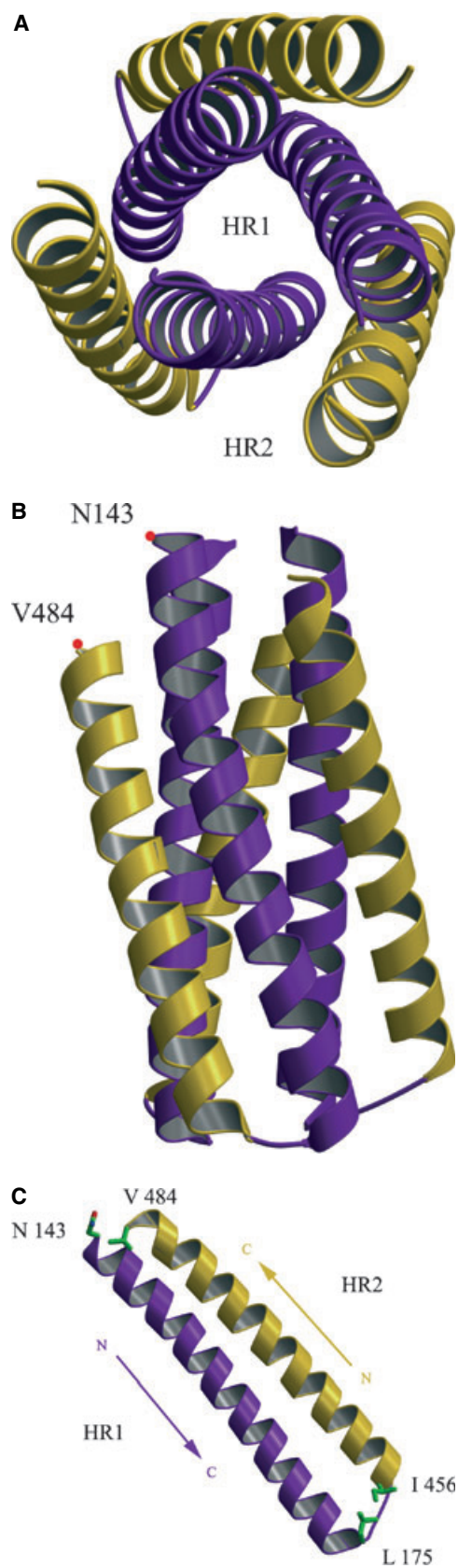
Interactions between HR1 and HR2

Three HR2 helices of the NiV fusion core pack against the outside of the central coiled-coil trimer in an obliquely antiparallel manner, which suggests a common interaction mode for the other well-studied Paramyxoviridae virus fusion proteins. The HR2 helices interact with HR1 mainly through hydrophobic interactions between hydrophobic residues in HR2 and the hydrophobic grooves on the surface of the central coiled coil (Fig. 3A). The interaction region of HR1 can be divided into three parts: the upper deep groove (I144–V158), the central shallow groove (V159–T164) and the lower deep groove (A165–L172) (Fig. 3B). Residues M463, I474, L481 and V484 of HR2 are anchored in the deep groove of HR1 and make a significant contribution to the hydrophobic interactions between HR1 and HR2 (Fig. 3B). Sequence comparison between NiV/HeV and other paramyxovirus fusion proteins shows that residues contributing to the HR1–HR2 interaction (e and g positions in HR1, a and d positions in HR2) are highly conserved (Figs 1B and 3B). This pattern of sequence conservation can also be shown by a helical wheel representation of one HR1 helix and one HR2 helix [21]. Sequence comparison between NiV and SV5 fusion proteins shows that five out of nine changes (including one A to V) occur in the e and g positions of HR1, and six out of nine changes (including two L to I and one I to V) occur in HR2 at the a and d positions. In contrast, only 13 out of 15 nonconservative changes occur at the outside f, b and c positions in HR1, and three out of 21 nonconservative changes occur at positions other than a and d in HR2 (Fig. 1B).

Comparison with other fusion proteins and a fusion core model for the Paramyxoviridae family

Among paramyxovirus fusion proteins, only the SV5 and human respiratory syncytial virus (hRSV) fusion core structures have been determined to date [32,37]. The NiV fusion core structure has a similar conformation to both SV5 F1 and hRSV, and can be superim-

Fig. 2. Overall views of the fusion core structure of Nipah virus (NiV). (A) Top view of the NiV F protein fusion core structure showing the three-fold axis of the trimer. (B) Side view of the NiV F protein fusion core structure showing the six-helix bundle. (C) Interactions between the termini of HR1 and HR2. HR1 and HR2 are represented by purple and golden ribbons, respectively. The interacting residues are shown as green sticks. The residues at the N-terminus and C-terminus are labeled.
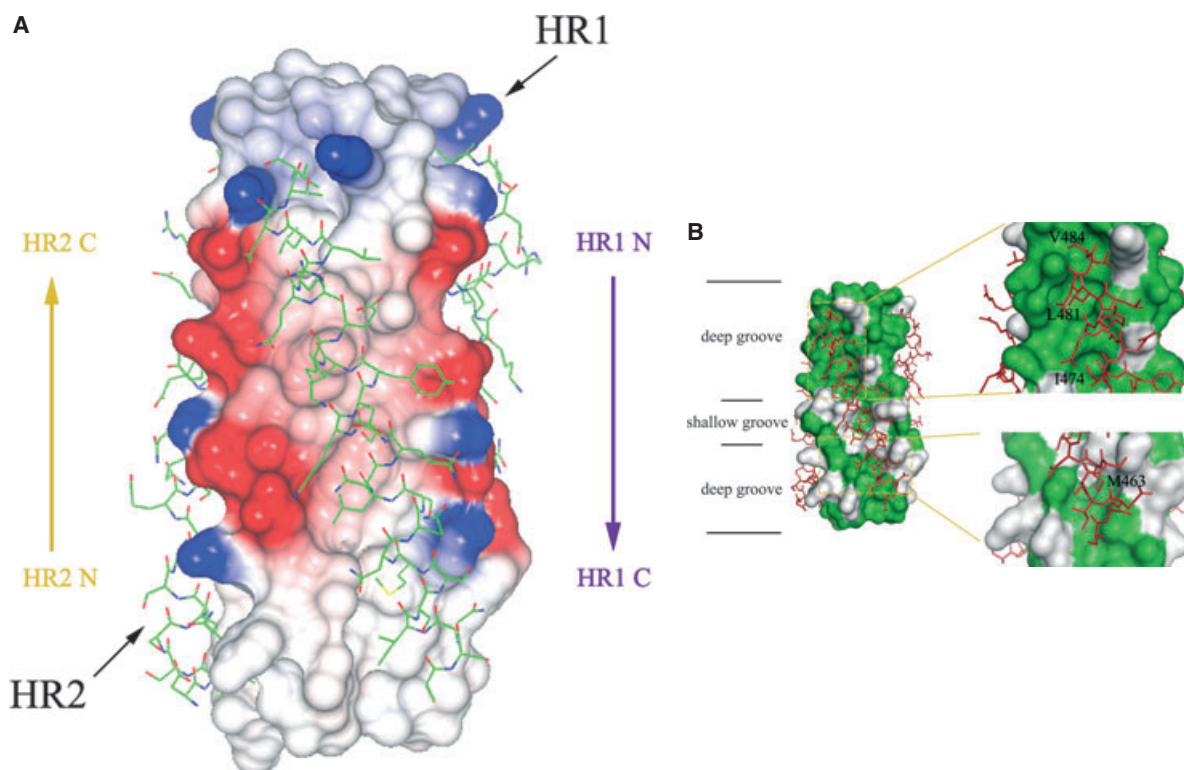
Fig. 3. The HR1–HR2 interactions. (A) A surface map showing the hydrophobic grooves on the surface of the Nipah virus (NiV) central coiled coil. Three HR2 helices pack against the hydrophobic grooves in an oblique antiparallel manner. The helical regions and extended regions in HR2 helices, which are represented by green sticks, can clearly be observed, and the boundaries of these regions are marked. (B) Details of the HR1–HR2 interaction in the NiV F protein fusion core. HR1 is shown in surface representation, and HR2 is represented by red sticks. The conserved residues are colored green, and all other residues are colored white. The two deep grooves, which are important for the HR1–HR2 interaction, are highlighted. The key residues and different parts of the HR1 surface are labeled.

posed with an rmsd of 0.68 Å and 0.67 Å between all Cα atoms, respectively. We will focus our structural comparison on NiV F and SV5 F, as the fusion core structures of hRSV and SV5 share significant similarity. Although the NiV and SV5 fusion cores share a very similar topology, they also have some significant differences.

First, the structure of the NiV F fusion core HR1 peptide (143–176) is much shorter than its counterpart in the SV5 fusion core (122–185), although HR2 has the almost same length in NiV (455–484) and SV5 (440–477) fusion cores (Fig. 4A,B). Second, the hydrophobic grooves on the surface of the central coiled coil have some significant differences, especially in the lower deep groove (Fig. 4C,D). In the structure of the NiV F fusion core, the lower deep groove formed by T164, A165, T168, V169 and L172 is much deeper than the equivalent region of the SV5 fusion core structure, formed by A157, T158, L161, G162 and V165 (Fig. 3E). This groove is so deep that we even observe that the bottom of the grooves are connected

to each other and form a connective hole in the HR1 surface. Residue M463, which occupies the d position in the HR2 region and faces the center of the trimer, anchors into this groove and greatly contributes to the stability of the fusion core complex. Residue L161 in the SV5 structure makes this groove more shallow than its counterpart, T168, in NiV due to the longer hydrophobic side chain. Sequence alignment with other Paramyxoviridae viruses also shows that NiV has the shortest hydrophobic residue in the T168 position and the longest residue in the M463 position.

Although they share many differences from other Paramyxoviridae fusion core proteins, the NiV and HeV F fusion cores also share certain similarities and show high conservation. Among the Paramyxoviridae, the NiV and HeV fusion cores have the shortest structures and sequences. However, all paramyxovirus fusion cores share the same core parts and are highly conserved, both in sequence (Fig. 1B) and in three-dimensional structure (Fig. 3B). These facts suggest that the structure of the NiV F fusion core may share
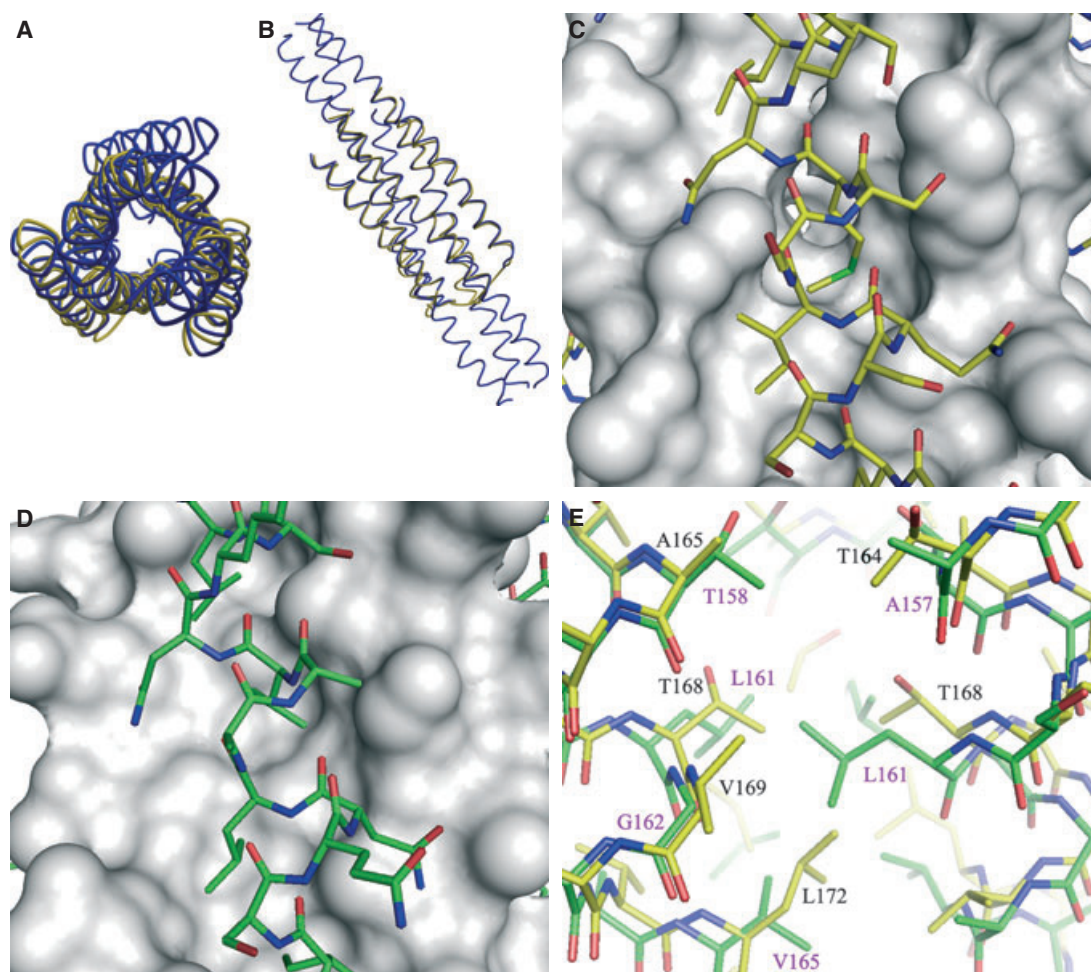
Fig. 4. A comparison between Nipah virus (NiV) and simian virus 5 (SV5) fusion core structures. (A) and (B) Top and side views showing the comparison between the NiV F fusion core and SV5 fusion core. The NiV F and SV5 fusion cores are represented as gold and blue Cα back-bone traces, respectively. (C) and (D) Comparison of the end deep groove positions in the NiV F and SV5 fusion cores. (A) The end deep groove on the surface of heptad repeat 1 (HR1) in the NiV F fusion core. HR1 is shown as a white molecular surface, and HR2 is represented by gold sticks. (B) The same orientation and position on the surface of HR1 in the SV5 fusion core. HR1 is shown as a white molecular surface, and HR2 is represented by green sticks. The position of the deep groove is highlighted by red lines. (E) Details of residues in the end deep grooves of the NiV F and SV5 fusion cores. NiV F fusion core residues are shown as yellow sticks with black labels; SV5 fusion core residues are shown as green sticks with purple labels.

common features with all Paramyxoviridae virus fusion cores, leading us to propose the NiV F fusion core structure as a model for Paramyxoviridae fusion cores. Furthermore, the conserved deep grooves at both ends of the NiV fusion core may provide a structural basis for the design of wide-spectrum therapeutics targeting the Paramyxoviridae family.

Conformational change and membrane fusion mechanisms

Structural studies of the influenza virus HA and HIV gp41 have established a paradigm for understanding the

mechanisms of viral and cellular membrane fusion [18]. The similarity between the NiV F protein and other widely studied viral fusion proteins, as well as previous biochemical analysis [38], indicates a similar mechanism of membrane fusion mediated by the NiV and HeV fusion proteins. The structures of the NiV and HeV fusion cores reported here add to the repertoire of paramyxovirus six-helix bundle fusion core structures, providing greater structural information in order to understand the formation of the fusion-active state of genus *Henipavirus*. Similar to SV5F and HIV gp41, the NiV and HeV fusion proteins probably undergo a series of conformational changes to become fusion-active. The

fusion loop, which inserts into the cellular membrane, is accepted to have the distinct conformational states proposed for the NiV F protein fusion core, including the native state, the prehairpin intermediate, and the fusion-active hairpin state. Several biological and inhibition studies have also provided good evidence that the fusion core in the crystal structure presented here is the final, stable form of the protein, which is the fusion-active state following one or more conformational changes. First, gel filtration and chemical crosslinking results demonstrated that the oligomeric state of the two-helix protein was a trimer. Even at high concentrations of the crosslinker, the monomer/dimer bands could be observed [31]. Second, NiV and HeV infection *in vitro* can be potently blocked by peptides corresponding to the C-terminal HR (HR2) of the HeV fusion envelope glycoprotein 39. These features suggest that the NiV F protein also undergoes a conformational change mechanism, similar to influenza HA and HIV gp41.

Inhibitors of NiV/HeV infection

As membrane fusion is a very important process during virus infection, inhibition studies have been carried out to find effective drugs to block virus infection by targeting the membrane fusion step. In the case of HIV-1, several strategies to block hairpin formation have been successfully developed to identify viral entry inhibitors that bind to the hydrophobic pocket and grooves on the surface of the central coiled coil consisting of HIV-1 gp41 N peptides. These useful viral entry inhibitors include D peptides, five-helix, and synthetic peptides derived from N or C peptides [40–42]. Successful viral entry inhibitors have also been identified for other viruses, such as T20 for HIV-1 and GP610 for Ebola virus. Analogous strategies could also be used for the design of NiV/HeV fusion inhibitors.

In 2005, several reports showed that NiV/HeV infection *in vitro* can be potently blocked by specific HR2 peptides. The improved second-generation HR2 peptides, which use poly(ethylene glycol) to facilitate peptide synthesis and increase solubility, also show good IC50 values in *in vitro* assays. The applied chemical modifications are also predicted to increase the serum half-life *in vivo* and should increase the chances of success in the development of an effective antiviral therapy [50]. The well-defined hydrophobic grooves on the surface of the central coiled coil of the NiV F protein fusion core identified from our structure can offer a reasonable explanation for the inhibition of NiV and HeV infection. Furthermore, the structures reported here provide significant targets for the design of NiV and HeV antiviral agents.

Experimental procedures

Purification and crystallization – the two-helix constructs of both NiV and HeV

Fusion proteins were prepared as a single chain by linking the HR1 and HR2 domains with an eight amino acid linker (GGSGGSGG). The PCR-directed gene was inserted into the pET22b vector (Novagen, Shanghai, China), and the target plasmids were transformed into BL21 (DE3) competent cells. The cells were cultured at 310 K in $2 \times$ YT medium containing 100 μg·mL^{-1} ampicillin and were induced with 0.2 mM isopropyl thio-β-D-galactoside (IPTG) when the culture density (D_{600}) reached 0.6–0.8. The selenomethinoine derivative HeV two-helix protein was expressed in M9 medium containing 30 mg·L^{-1} selenomethionine in *E. coli* strain BL21 (DE3). The two products were both purified by nickel-nitrilotriacetic acid affinity chromatography followed by gel filtration chromatography. The purified NiV two-helix and HeV two-helix derivative were dialyzed against crystallization buffer (10 mM Tris/HCl, pH 8.0, 10 mM NaCl) and concentrated to 10–15 mg·mL^{-1}. Initial crystallization conditions were screened using Crystal Screen reagent kits I and II (Hampton Research, Aliso Viejo, CA, USA) and a poly(ethylene glycol) screening kit prepared in-house.

Good-quality NiV two-helix crystals were obtained from 0.1 M Tris/HCl (pH 8.5)/29% poly(ethylene glycol) 4000 (v/v). Good-quality HeV two-helix derivative crystals were obtained from 0.1 M Hepes (pH 6.5)/10% poly(ethylene glycol) 4000 (v/v). The preparation and crystallization of the two-helix proteins of NiV and HeV have previously been reported in detail [21].

Data collection and processing

Data collection from the NiV two-helix crystal was performed in-house on a Rigaku RU200 (Tokyo, Japan) rotating-copper-anode X-ray generator operated at 48 kV and 98 mA (CuKα; $\lambda = 1.5418$ Å) with an Mar345 image-plate detector. The crystal was mounted on nylon loops and flash-cooled in a cold nitrogen gas stream at 100 K using an Oxford Cryosystems (Oxford, UK) cold stream and with the reservoir solution as cryoprotectant. Data were indexed and scaled using the HKL2000 programs DENZO and SCALEPACK [43]. The HeV two-helix selenomethionine derivative crystal was mounted on nylon loops and flash-frozen in a cold nitrogen gas stream at 100 K using an Oxford Cryosystems cold stream and with 0.1 M Hepes (pH 6.5)/25% poly(ethylene glycol) 400 as cryoprotectant. MAD data were collected by a rotation method using a Mar CCD detector with synchrotron radiation beamline 3W1A of the Beijing Synchrotron Radiation Facility. Data were collected from a single selenomethionyl derivative crystal at peak (0.9799 Å), edge (0.9801 Å) and

remote (0.9500 Å) wavelengths to 2.2 Å. Data were indexed and scaled using DENZO and SCALEPACK programs [43].

Phase determination and model refinement

For determination of the HeV two-helix structure, initial MAD phasing steps were performed using SOLVE [44], and density modification was performed using RESOLVE [45]. The program O [36] was used for manual tracing of the experimental density map, and the initial structure was subsequently refined using the programs O [36] and CNS [35]. The NiV two-helix structure was determined by molecular replacement with the HeV two-helix structure as a search model. Rotation and translation function searches were performed with the program CNS [35]. The model was further improved by manual building and refinement using the programs O [36] and CNS [35]. The quality of the two structures was verified by PROCHECK [46], with none of the main-chain torsion angles located in disallowed regions of the Ramachandran plot. Structure determination and refinement statistics are summarized in Table 1. The figures were generated with the programs GRASP [47], PYMOL [47] and MOLSCRIPT [48].

Accession codes

Coordinates and structure factors for the NiV and HeV fusion core crystal structures have been deposited in the RCSB PDB with accession numbers 1WP7 and 1WP8, respectively.

Acknowledgements

References

1 Chua KB, Goh KJ, Wong KT, Kamarulzaman A, Tan PS, Ksiazek TG, Zaki SR, Paul G, Lam SK & Tan CT (1999) Fatal encephalitisdue to Nipah virus among pig-farmers in Malaysia. *Lancet* **354**, 1257–1259.

2 Chua KB, Bellini WJ, Rota PA, Harcourt BH, Tamin A, Lam SK, Ksiazek TG, Rollin PE, Zaki SR, Shieh W *et al.* (2000) Nipah virus: a recently emergent deadly paramyxovirus. *Science* **288**, 1432–1435.

3 Enserink M (2004) Emerging infectious diseases. Nipah virus (or a cousin). strikes again. *Science* **303**, 1121.

4 Murray K, Rogers R, Selvey L, Selleck P, Hyatt A, Gould A, Gleeson L, Hooper P & Westbury H (1995) A novel morbillivirus pneumonia of horses and its transmission to humans. *Emerg Infect Dis* **1**, 31–33.

5 Mackenzie JS, Chua KB, Daniels PW, Eaton BT, Field HE, Hall RA, Halpin K, Johansen CA, Kirkland PD,

Lam SK *et al.* (2001) Emerging viral diseases of Southeast Asia and the Western Pacific. *Emerg Infect Dis* **7**, 497–504.

6 Wang LF & Eaton BT (2001) Emerging Paramyxoviruses. *Infect Disease Rev Microbs Man, Animals Environ* **3**, 52–69.

7 Wang LF, Yu M, Hansson E, Pritchard LI, Shiell B, Michalski WP & Eaton BT (2000) The exceptionally large genome of Hendra virus: support for creation of a new genus within the family Paramyxoviridae. *J Virol* **74**, 9972–9979.

8 Chan YP, Chua KB, Koh CL, Lim ME & Lam SK (2001) Complete nucleotide sequences of Nipah virus isolates from Malaysia. *J Gen Virol* **82**, 2151–2155.

9 Lam SK (2003) Nipah virus − a potential agent of bioterrorism? *Antiviral Res* **57**, 113–119.

10 Lamb RA, Collins PL, Kolakofsky D, Melero JA, Nagai Y, Oldstone MBA, Pringle CR & Rima BK (2000) Paramyxoviridae. In *Virus Taxonomy: Classification and Nomenclature of Viruses, 7th Report* (vanRegenmortel MHV, Fauquet CM, Bishop DHL, Carstens EB, Estes MK, Lemon SM, Maniloff J, Mayo MA, McGeoch DJ, Pringle CR & Wickner RB, eds), pp. 549–561. Academic Press, San Diego.

11 Chang P-C, Hsieh M-L, Shien J-H, Graham DA, Lee M-S & Shieh HK (2001) Complete nucleotide sequence of avian paramyxovirus type 6 isolated from ducks. *J Gen Virol* **82**, 2157–2168.

12 Bossart KN, Wang LF, Eaton BT & Broder CC (2001) Functional expression and membrane fusion tropism of the envelope glycoproteins of Hendra virus. *Virology* **290**, 121–135.

13 Tamin A, Harcourt BH, Ksiazek TG, Rollin PE, Bellini WJ & Rota PA (2002) Functional properties of the fusion and attachment glycoproteins of Nipah virus. *Virology* **296**, 190–200.

14 Lamb RA (1993) Paramyxovirus fusion: a hypothesis for changes. *Virology* **197**, 1–11.

15 Lamb RA, Joshi SB & Dutch RE (1999) The paramyxovirus fusion protein forms an extremely stable core trimer: structural parallels to influenza virus haemagglutinin and HIV-1 gp41. *Mol Membr Biol* **16**, 11–19.

16 Eckert DM & Kim PS (2001) Mechanisms of viral membrane fusion and its inhibition. *Annu Rev Biochem* **70**, 777–810.

17 Weissenhorn W, Dessen A, Calder LJ, Harrison SC, Skehel JJ & Wiley DC (1999) Structural basis for membrane fusion by enveloped viruses. *Mol Membr Biol* **16**, 3–9.

18 Bentz J (2000) Membrane fusion mediated by coiled coils: a hypothesis. *Biophys J* **78**, 886–900.

19 Skehel JJ & Wiley DC (1998) Coiled coils in both intracellular vesicle and viral membrane fusion. *Cell* **95**, 871–874.

20 Skehel JJ & Wiley DC (2000) Receptor binding and membrane fusion in virus entry: the influenza hemagglutinin. *Annu Rev Biochem* **69**, 531–569.

21 Xu Y, Gao S, Cole DK, Zhu J, Su N, Wang H, Gao F & Rao Z (2004) Basis for fusion inhibition by peptides: analysis of the heptad repeat regions of the fusion proteins from Nipah and Hendra viruses, newly emergent zoonotic paramyxoviruses. *Biochem Biophys Res Commun* **315**, 664–670.

22 Skehel JJ, Cross K, Steinhauer D & Wiley DC (2001) Influenza fusion peptides. *Biochem Soc Trans* **29**, 623–626.

23 Lu M, Blacklow SC & Kim PS (1995) A trimeric structural domain of the HIV-1 transmembrane glycoprotein. *Nat Struct Biol* **2**, 1075–1082.

24 Chan DC & Kim PS (1998) HIV entry and its inhibition. *Cell* **93**, 681–684.

25 Cuzin L & Alvarez M (2003) Enfuvirtide for prophylaxis against HIV infection. *N Engl J Med* **349**, 2169–2170.

26 Bossart KN, Wang LF, Flora MN, Chua KB, Lam SK, Eaton BT & Broder CC (2002) Membrane fusion tropism and heterotypic functional activities of the Nipah virus and Hendra virus envelope glycoproteins. *J Virol* **76**, 11186–11198.

27 Zhu J, Zhang CW, Qi Y, Tien P & Gao GF (2002) The fusion protein core of measles virus forms stable coiled-coil trimer. *Biochem Biophys Res Commun* **299**, 897–902.

28 Zhu JQ, Zhang CW, Rao Z, Tien P & Gao GF (2003) Biochemical and biophysical analysis of heptad repeat regions from the fusion protein of Menangle virus, a newly emergent paramyxovirus. *Arch Virol* **148**, 1301–1316.

29 Zhu J, Li P, Wu T, Gao F, Ding Y, Zhang CW, Rao Z, Gao GF & Tien P (2003) Design and analysis of post-fusion 6-helix bundle of heptad repeat regions from Newcastle disease virus F protein. *Protein Eng* **16**, 373–379.

30 Zhu J, Ding Y, Gao F, Wu T, Zhang CW, Tien P, Rao Z & Gao GF (2003) Crystallization and preliminary X-ray crystallographic analysis of the trimer core from measles virus fusion protein. *Acta Crystallogr D Biol Crystallogr* **59**, 587–590.

31 Yu M, Wang E, Liu Y, Cao D, Jin N, Zhang CW, Bartlam M, Rao Z, Tien P & Gao GF (2002) Six-helix bundle assembly and characterization of heptad repeat regions from the F protein of Newcastle disease virus. *J Gen Virol* **83**, 623–629.

32 Wang E, Sun X, Qian Y, Zhao L, Tien P & Gao GF (2003) Both heptad repeats of human respiratory syncytial virus fusion protein are potent inhibitors of viral fusion. *Biochem Biophys Res Commun* **302**, 469–475.

33 Li PY, Zhu JQ, Wu BL, Gao F, Tien P, Rao Z & Gao GF (2003) Crystallization and preliminary X-ray diffraction analysis of post-fusion six-helix bundle core structure from Newcastle disease virus F protein. *Acta Crystallogr D Biol Crystallogr* **59**, 1296–1298.

34 Singh M, Berger B & Kim PS (1999) LearnCoil-VMF: computational evidence for coiled-coil-like motifs in many viral membrane-fusion proteins. *J Mol Biol* **290**, 1031–1041.

35 Brunger AT, Adams PD, Clore GM, DeLano WL, Gros P, Grosse-Kunstleve RW, Jiang JS, Kuszewski J, Nilges M, Pannu NS *et al.* (1998) Crystallography and NMR system: a new software suite for macromolecular structure determination. *Acta Crystallogr D Biol Crystallogr* **54**, 905–921.

36 Jones TA, Zou JY, Cowan SW & Kjeldgaard M (1991) Improved methods for building protein models in electron density maps and the location of errors in these models. *Acta Crystallogr A* **47**, 110–119.

37 Baker KA, Dutch RE, Lamb RA & Jardetzky TS (1999) Structural basis for paramyxovirus-mediated membrane fusion. *Mol Cell* **3**, 309–319.

38 Liu Y, Zhu J, Feng MG, Tien P & Gao GF (2004) Six-helix bundle assembly and analysis of the central core of mumps virus fusion protein. *Arch Biochem Biophys* **421**, 143–148.

39 Bossart KN, Mungall BA, Crameri G, Wang LF, Eaton BT & Broder CC (2005) Inhibition of Henipavirus fusion and infection by heptad-derived peptides of the Nipah virus fusion glycoprotein. *Virol J* **2**, 57.

40 Eckert DM & Kim PS (2001) Design of potent inhibitors of HIV-1 entry from the gp41 N-peptide region. *Proc Natl Acad Sci USA* **98**, 11187–11192.

41 Eckert DM, Malashkevich VN, Hong LH, Carr PA & Kim PS (1999) Inhibiting HIV-1 entry: discovery of D-peptide inhibitors that target the gp41 coiled-coil pocket. *Cell* **99**, 103–115.

42 Root MJ, Kay MS & Kim PS (2001) Protein design of an HIV-1 entry inhibitor. *Science* **291**, 884–888.

43 Otwinowski Z & Minor W (1997) Processing of x-ray diffraction data collected in oscillation mode. *Methods Enzymol* **276**, 307–326.

44 Terwilliger TC & Berendzen J (1999) Automated MAD and MIR structure solution. *Acta Crystallogr D Biol Crystallogr* **55**, 849–861.

45 Terwilliger TC (2001) Maximum-likelihood density modification using pattern recognition of structural motifs. *Acta Crystallogr D Biol Crystallogr* **57**, 1755–1762.

46 Laskowski RA, MacArthur MW, Moss DS & Thornton JM (1993) PROCHECK: a program to check the stereochemical quality of protein structures. *J Appl Crystallogr* **26**, 283–291.

47 Nicholls A, Sharp KA & Honig B (1991) Protein folding and association: insights from the interfacial and thermodynamic properties of hydrocarbons. *Proteins* **11**, 281–296.

48 Kraulis PJ (1991) MOLSCRIPT: a program to produce both detailed and schematic plots of protein structures. *J Appl Crystallogr* **24**, 946–950.